Random lasing of $CsPbBr_3$ perovskite thin films pumped by modulated electron beam

Haibo Fan (樊海波)[1], Yining Mu (母一宁)[1,*], Chunyang Liu (刘春阳)[1,2,], Yan Zhu (朱 焱)[1], Guozhen Liu (刘国桢)[1], Shuai Wang (王 帅)[1], Yanzheng Li (李彦正)[1], and Peng Du (杜 鹏)[1]**

[1]*School of Science, Changchun University of Science and Technology, Changchun 130022, China*
[2]*Centre for Advanced Optoelectronic Functional Materials Research and Key Laboratory of UV-Emitting Materials and Technology (Northeast Normal University), Ministry of Education, Changchun 130024, China*
**Corresponding author: muyining1985@163.com; **corresponding author: liucy169@nenu.edu.cn*
Received August 21, 2019; accepted September 25, 2019; posted online December 10, 2019

Aiming at the application requirements of information optics, this Letter proposed a perovskite quantum dot random lasing pumping method suitable for high-speed modulation. At the same time, the luminescence characteristics of perovskite quantum dot films under electron beam pumping conditions are analyzed, and the random lasing mechanism of electron beam pumping $CsPbBr_3$ quantum dot films is revealed. Finally, it is confirmed that perovskite quantum dots are easy to realize random lasing under electron beam pumping conditions.

Keywords: perovskite; quantum dots; electron beam; random laser.
doi: 10.3788/COL202018.011403.

With the rapid development of visible light communication technology, light sources with instantaneous high-power output characteristics have become the main technical limitations[1–3]. With higher quantum yield, lower threshold lasing, and better transient optical characteristics to be realized in new-type light source, lighting communication technology will have further promotion[4–6]. In 2015, Zeng *et al.* firstly reported a trichromatic electroluminescent diode based on all-inorganic perovskite quantum dots[7]; the low threshold stimulated emission of all-inorganic colloidal perovskite quantum dots is realized[8]. In the same year, *Nature Communications* reported the work of using nanocrystalline structures to realize the optically pumped random laser of perovskite quantum dots[9]. In 2018, *Nature* firstly reported the perovskite LED with external quantum efficiency of 20%[10,11]. Therefore, the perovskite quantum dots have a better quantum yield and an extremely lower optical lifetime, which are currently very suitable transient light-emitting semiconductor material for achieving visible light illumination communication[12–14]. In 2018, Yuan *et al.* of Xi'an Jiaotong University discussed the feasibility of injection electroluminescent laser of all-inorganic perovskite materials[15]. In order to satisfy the power requirements of the illumination, a wider cross-sectional area of a diode is the prerequisite for obtaining a high-current output. However, semiconductor-wise, the junction capacitance in the positive-intrinsic-negative (PIN) structure of the injection electroluminescent quantum dot source is proportional to its cross-sectional area, which constrains the transient optical characteristics and power output capability of quantum dot light source theoretically.

Currently, optical pumping lasing effects based on perovskite quantum dots are much better than other pumping methods. As early as 2016, some reports showed an optical pump lasing with half-width of less than 0.1 nm and quality factor of more than 5000[16]. As a pumping method with high research value, optical pumping is not conducive to device integration, and, for perovskite quantum dot pumping, it needs shorter wavelength and higher-energy photon drive, so it is extremely difficult to be widely used in commercial fields. Since the electron beam pumping mode is very similar to the optical pumping mode, we proposed to use the electron beam pumping mode to realize the modulated pump lasing. Aiming at information optics requirements, an electron beam pumping random laser based on $CsPbBr_3$ quantum dot is realized, which verifies feasibility and high efficiency of perovskite quantum dot films pumped by an electron beam.

The specific process of $CsPbBr_3$ quantum dot films is as follows: as shown in Fig. 1, $CsPbBr_3$ quantum dots were synthesized in an oil phase protected by an inert gas using caesium oleate and lead bromide as precursors by thermal injection and rapid ion exchange. After centrifugation and purification by high-speed centrifuge, the $CsPbBr_3$ quantum dot solution of all-inorganic metals with hexane as the

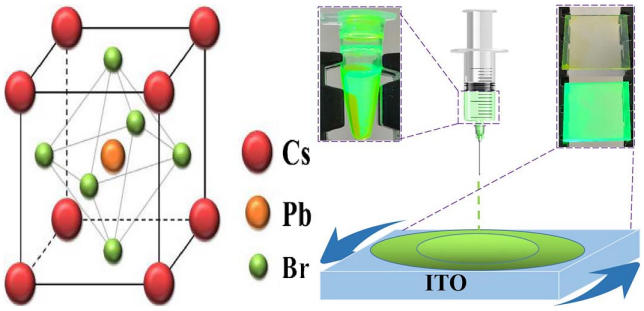

Fig. 1. Crystal structure and thin film preparation process of $CsPbBr_3$.

solvent and a concentration of 10 mg/mL emitting green fluorescence was prepared. The conductive glass [indium tin oxide (ITO)] substrate was ultrasonically cleaned with acetone, absolute ethanol, and deionized water for 15 min, dried by a nitrogen gun, and placed in a drying oven at 80°C for 30 min. The prepared quantum dot solution was uniformly stirred by a magnetic stirrer to obtain a yellow transparent $CsPbBr_3$ quantum dot spin coating solution. Then, the glue machine was used. The quantum dot spin coating solution obtained by one-step spin coating method is dropped on a conductive glass substrate through a special syringe, where the homogenizing speed of 900 r/min is maintained for 5–10 s before dripping, and the homogenizing speed of 3500 r/min is maintained after dripping 10–20 s. Finally, spin coating resulted in a uniformly translucent $CsPbBr_3$ quantum dot film. The amount of syringe droplets was determined by means of a microelectronic analytical balance with a reading accuracy of 0.01 mg. The experiment shows that under certain conditions, the higher the spin coating speed, the longer the gelling time, and the thinner the quantum dot film.

The X-ray diffraction pattern of $CsPbBr_3$ quantum dots is shown in Fig. 2. The characteristic peaks are 15.1°, 21.5°, 30.4°, 34.2°, and 37.6°, respectively, corresponding to crystal structures {001}, {110}, {002}, {210}, and {211}, consistent with the standard diffraction pattern obtained from the Joint Committee on Powder Diffraction Standards (JCPDS) database (No. 01-072-7929), belonging to cubic crystal structure (Fig. 1). In addition, we characterized the $CsPbBr_3$ nanocrystals by transmission electron microscopy (TEM). As shown in Fig. 3(a), the $CsPbBr_3$ nanocrystalline morphology effect used herein is shown. Figure 3(b) shows the size distribution of the nanocrystals, which show that the average size of the nanocrystals is about 15 nm. Figures 3(c)–3(g) represent scanning electron microscope images of $CsPbBr_3$ quantum dot films with different spin coating thicknesses separately.

As a vacuum electron multiplier device with continuous dynode, the microchannel plate has sub-nanosecond

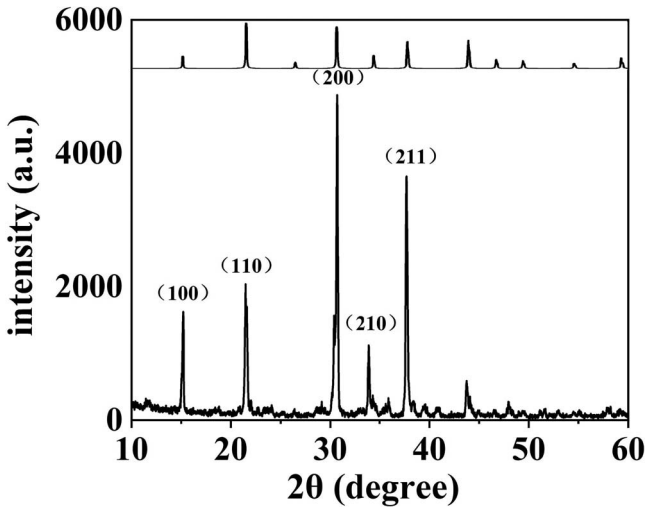

Fig. 2. X-ray diffraction patterns of $CsPbBr_3$ nanocrystals.

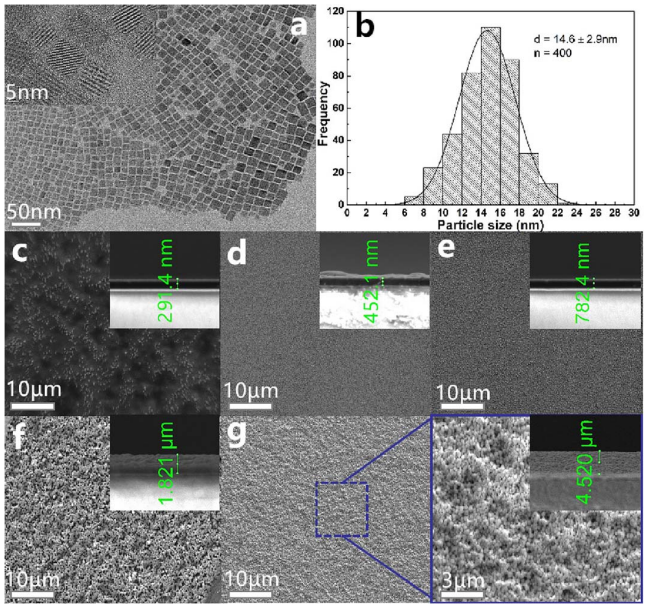

Fig. 3. (a) TEM characterization of $CsPbBr_3$ nanocrystals. (b) The size distribution of the nanocrystals. (c)–(g) Scanning electron microscopy (SEM) characterization of $CsPbBr_3$ perovskite thin films with thicknesses of 300, 450, 800, 1800, and 4500 nm.

frequency response characteristics and high gain capability, which makes it widely used in range-gated imaging and transient optics field and very suitable for high-speed modulation. In this Letter, a seed light source is used as external trigger modulation to drive photoelectrodes to produce photoelectrons, and the photoelectrons take advantage of microchannel plates to achieve power multiplication and yield high-energy electron beams. Finally, the beam driven by a strong electric field is used to bombard the $CsPbBr_3$ thin film. The concrete devices are shown in Fig. 4.

An ultraviolet semiconductor LED with a wavelength of 375 nm and an output power of 0.5 mW is used as an

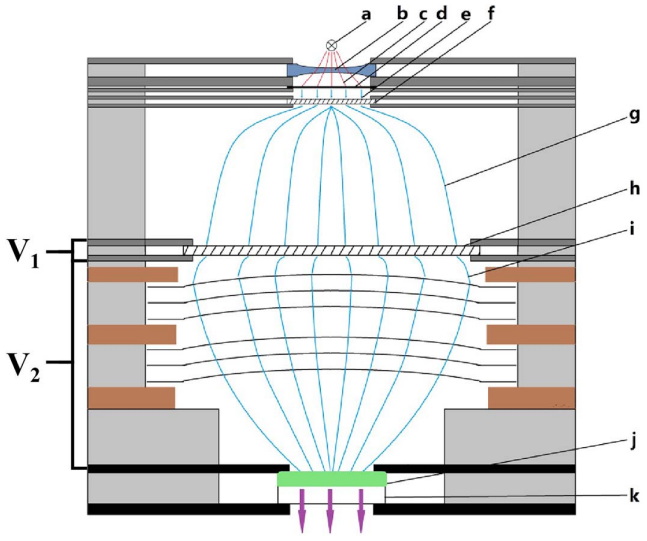

Fig. 4. Schematic diagram of electron beam pumping source.

external trigger source a. The modulated light pulse c emitted by a is uniformly irradiated to the photocathode d after passing through the beam expanding optical system b. Photocathode d is a gold film with a thickness of 100 nm. The modulated light pulse c is converted to electron pulse e through photocathode d. Electron pulse e generates pulse electron beam g through microchannel plate f with high gain and low power output. The pulsed electron cloud g is uniformly covered on the incident surface of the low gain, high-power output microchannel plate h. The electrons output from the outgoing surface are accelerated at subsequent high voltage to form high-energy electron beam i. The high-energy electron beam i is focused on the surface of $CsPbBr_3$ quantum dot thin film j under the action of a three-stage electronic optical focusing system. The optical quartz ITO was selected as the substrate of the quantum dot film k, and the conductive layer of k was used as the anode of the whole electronic optical system. We effectively controlled the gain characteristic by exactly changing the voltage V_1 across the h and thus effectively controlling the current value of i. The bombardment potential energy of i is directly determined by controlling the voltage V_2 between the surface electrode film of h and the conductive layer of k. Thus, by adjusting V_1 and V_2, the pump energy of the final electron beam on the quantum dot film can be directly fine-tuned. In this Letter, $CsPbBr_3$ quantum dot film is used as the active film for luminescence.

In the experiment, the spectrum was measured by the SD1220-V spectrometer of OTO Photonics Company with the resolution of 0.68 nm. The $CsPbBr_3$ quantum dot film was excited by continuous ultraviolet light at 365 nm, and the spectra obtained at different excitation power densities are shown in Fig. 5, which show that the emission peak is located at 520 nm, and full width at half-maximum (FWHM) is 20 nm. Subsequently, we placed the $CsPbBr_3$ quantum dot film assembled according to the device structure of Fig. 4 into a vacuum test system. V_2 bombards the $CsPbBr_3$ quantum dot film with 0.5 kV, 2 kV, 3 kV, 4 kV,

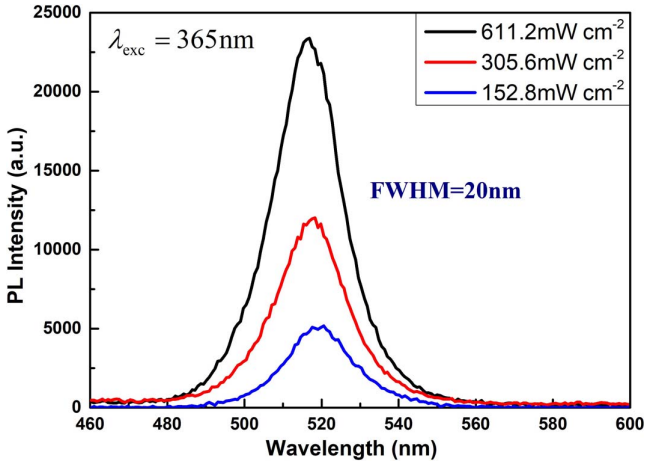

Fig. 5. Photoluminescence spectra of $CsPbBr_3$ quantum dot thin films.

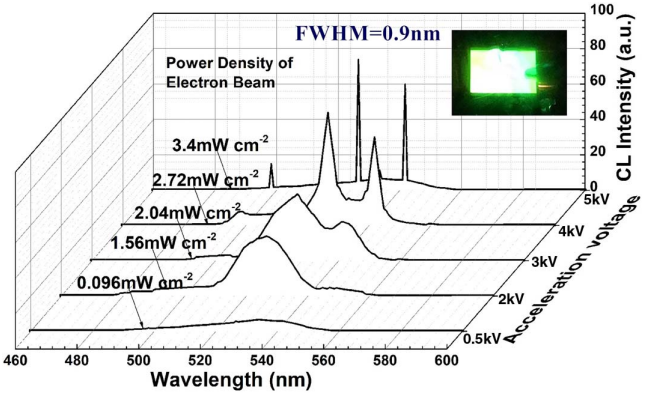

Fig. 6. Electron beam pumping spectra of $CsPbBr_3$ quantum dot thin films by different acceleration voltages.

and 5 kV accelerated electron beam, and the changes of the radiation spectrum are shown in Fig. 6. By controlling V_1, i is maintained at around 600 nA. When V_2 is 0.5 kV, the radiant light exhibits a broad spontaneous emission spectrum. With V_2 increasing, the area near the center of the gain curve is preferentially amplified, indicating that the portion of the line width is significantly narrowed, and lasing is formed. When V_2 exceeds a certain threshold (3 kV), a spike appears in the emission spectrum. When V_2 is further increased to 5 kV, a narrower peak appears, as shown in Fig. 6. At this time, the FWHM of the lasing is 1 nm or less, which is 1/20 of the half-width of the photoluminescence of the quantum dot film of Fig. 5.

It can be seen from Fig. 6 that the number of resonance peaks of the lasing increases with the electron beam pumping power, and the resonance mode pitch is not uniform, which is a characteristic of a typical random laser mode[17,18]. Moreover, the random laser does not need to add a resonant cavity, which confirms the feasibility of electron beam pumping $CsPbBr_3$ quantum dot gain dielectric film random lasing.

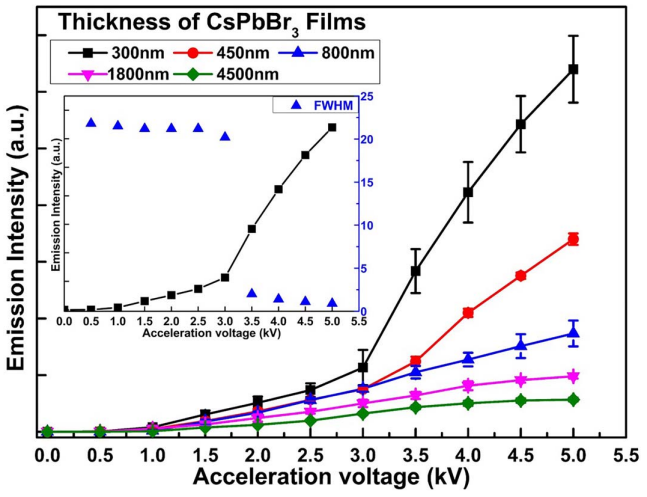

Fig. 7. Luminescence intensity of $CsPbBr_3$ quantum dots with different film thicknesses pumped by an electron beam. The inset shows the lasing threshold and FWHM variation of the 300 nm $CsPbBr_3$ quantum dot film.

In addition, we have carried out electron beam pump experiments on different thickness $CsPbBr_3$ quantum dot films. According to the vacuum pumping structure show in Fig. 4, when V_2 is 5 kV, the transmittance of the quantum dot film is measured by a spectrometer placed under the ITO substrate k, as shown in Fig. 7. We discovered that the electron beam pumping effect of the thin film with a thickness of 300 nm is obvious, and, with the increase of the thickness of the thin film, the light intensity decreases, and the lasing threshold increases, until the lasing does not occur. The inset of Fig. 7 shows the lasing threshold and FWHM variation of the 300 nm $CsPbBr_3$ quantum dot film. When V_2 is 500 V, the lower surface of the quantum dot film begins to emit light. When the bombardment voltage increases to 3 kV, the output power increases greatly, the radiation spectrum has a narrow peak, and the FWHM becomes smaller.

Based on the above experimental results, the random lasing mechanism of electron beam pumped $CsPbBr_3$ quantum dot films is analyzed and discussed as follows.

It is pointed out in Refs. [19,20] that the optically pumped lasing relies on the excitation beam to realize the particle beam inversion to produce excitation light, and the excitation light is scattered randomly inside the quantum dot. When the scattering is strong enough, continuous multiple scattering makes it possible for photons to return to the original scattering point or to form a feedback loop (ring cavity), which shapes local resonance of light and produces a random laser[19,20]. The electron beam pumping of perovskite quantum dots is very similar to optical pumping. The available kinetic energy of an electron beam in a vacuum environment is much higher than that of a solid, which makes the scattering trajectory of high-energy electrons in the three-dimensional fluorescence layer more random. Therefore, the process of an electron beam transmitting a quantum dot thin film depending on its own kinetic energy has a very strong random scattering characteristic, which largely replaces the scattering centers in the gain medium and enhances multiple scattering of light. As shown in Fig. 8, the probability of forming a ring cavity inside the gain medium is further increased by continuous multiple strong scattering, which makes it easier to lead random lasers.

Besides, different from the optical pumping mode, perovskite quantum dot electron beam pumping is a typically complex process. As shown in Fig. 8, after the high-energy electron beam enters the quantum dot film, the kinetic energy carried by the electron beam itself will gradually decrease with the depth of incidence, which causes the formation of multiple scattering and ring cavities at the incident surface to be much larger than that at the bottom of the film. Simulated by CASINO software, Fig. 9 shows the simulated energy distribution of the electron beam inside the quantum dot film. There is energy loss in the process of high-energy electron beam transmission through the active film. With the deepening of transmission, the kinetic energy of electrons decays and the scattering intensity of electrons decreases. The results of transmission spectrum measurement are shown in Fig. 7. The electrons have strong kinetic energy at the surface of the fluorescent layer, which leads to more obvious random scattering and is easier to produce a random laser. Therefore, when the thickness of the quantum dot thin film is 300 nm, the lasing effect measured on the back of ITO is the best. With the increase of the thickness of the film, although there is a laser on the surface of the fluorescent layer, the scattering intensity decreases due to the attenuation of the electronic kinetic energy of the lower layer, which leads to the lower layer mainly relying on electric field recombination luminescence. Therefore, with the increase of the film thickness, the intensity of the back of ITO decreases, and the laser threshold increases, which is an unsatisfied laser condition. Even when the film thickness is too thick, it is extremely difficult to measure the spectrum.

It can be seen that perovskite quantum dots are easier to realize random maser under the condition of electron beam pumping. As shown in Fig. 7, that thickness of the film directly affects the distribution of the kinetic energy of the electron beam in the three-dimensional fluorescent layer, which directly affected the light intensity

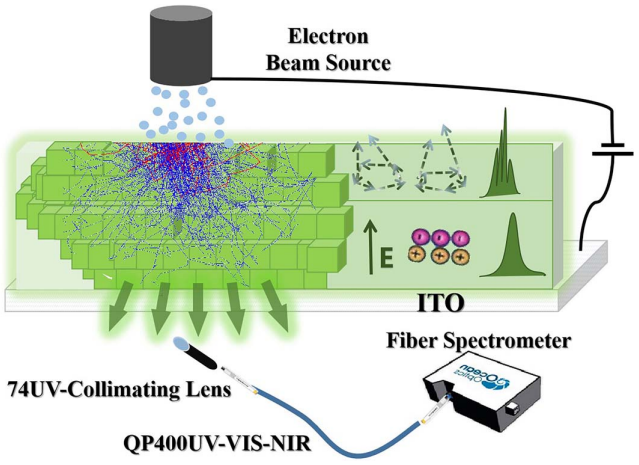

Fig. 8. Schematic diagram of random lasing mechanism of electron beam pumped $CsPbBr_3$ quantum dots.

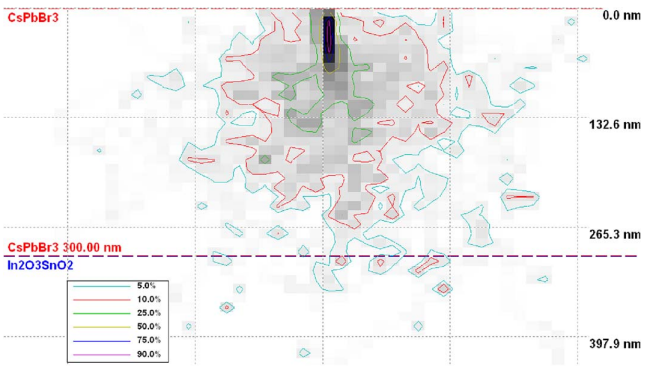

Fig. 9. Energy distribution of the electron beam inside the quantum dot films.

and the threshold of the back transmission-type measurement of perovskite quantum dots.

This Letter proposed a pumping method suitable for perovskite quantum dot modulation lasing, revealing the transient lasing properties of perovskite quantum dots under modulated electron beam pumping. The random lasing mechanism in the electron beam pumping mode is analyzed and discussed. The conclusion is as follows. Firstly, the mechanism of electron beam pumping is distinct from that of optical pumping in terms of the luminescence of perovskite quantum dot films. The high-energy electron beam has very strong random scattering characteristics, which makes it easier to achieve random lasing. Secondly, compared to the optical pump lasing of the perovskite quantum film, the electron beam pumping lasing makes it easier to achieve high-speed modulation, thereby producing an optoelectronic device having information-carrying capability. Thirdly, compared to electro-injected perovskite quantum dot luminescence, electron beam pumping has higher kinetic energy. The thermal effect caused by high-current injection can be effectively avoided by increasing the acceleration voltage. In particular, it can be more subtle to avoid the mutual limitation between the frequency response characteristics and the power characteristics of the junction capacitance in the diode structure, which fully embodies the great advantages of low recombination lifetime of the perovskite quantum dot carriers and high fluorescence quantum yield.

The experimental results obtained in this Letter are combined with the analysis and discussion of the random lasing mechanism. At present, we believe that it has a very broad prospect to realize information light source devices by using an electron beam to pump perovskite quantum dots. The research team will further explore the self-saturation mechanism of electron beam pumping lasing of perovskite quantum dots so as to improve the life of light source devices.

This work was supported by the National Natural Science Foundation of China (NSFC) (Nos. 51602028, 61905026, and 11874091), the Jilin Province Science and Technology Development Project (Nos. 20180519019JH and 20180804009HJ), the Jilin Province Industrial Innovation Special Fund Project (Nos. 2018C040-3 and 2019C043-6), the Development of Key Laboratory of Astronomical Optics Technology, the Chinese Academy of Sciences (No. CAS-KLAOT-KF201803), and the Changchun University of Science and Technology (No. XJJLG-2017-01).

References

1. H. Harald, L. Yin, Y. Wang, and C. Chen, J. Lightwave Technol. **34**, 1533 (2015).
2. H. Li, X. Chen, J. Guo, and H. Chen, Opt. Express **22**, 27203 (2014).
3. K. Ho, R. Chen, G. Liu, C. Shen, J. Holguin-Lerma, A. Al-Saggaf, T. Ng, M. Alouini, J. He, and B. Ooi, Opt. Express **26**, 3037 (2018).
4. L. Protesescu, S. Yakunin, M. Bodnarchuk, F. Krieg, R. Caputo, C. Hendon, R. Yang, A. Walsh, and M. Kovalenko, Nano Lett. **15**, 3692 (2015).
5. K. Lee, Ch. Han, H. Kang, H. Ko, Ch. Lee, J. Lee, N. Myoung, S. Yim, and H. Yan, ACS Nano **9**, 10941 (2015).
6. Y. Cao, N. Wang, H. Tian, J. Guo, Y. Wei, H. Chen, Y. Miao, W. Zou, K. Pan, Y. He, H. Cao, Y. Ke, M. Xu, Y. Wang, M. Yang, K. Du, Z. Fu, D. Kong, D. Dai, Y. Jin, G. Li, H. Li, Q. Peng, J. Wang, and W. Huang, Nature **562**, 249 (2018).
7. J. Song, J. Li, X. Li, L. Xu, Y. Dong, and H. Zeng, Adv. Mater. **27**, 7161 (2015).
8. Y. Wang, X. Li, J. Song, L. Xiao, H. Zeng, and H. Sun, Adv. Mater. **27**, 7101 (2015).
9. S. Yakunin, L. Protesescu, F. Krieg, M. Bodnarchuk, G. Nedelcu, M. Humer, G. Luca, M. Fiebig, W. Heiss, and M. Kovalenko, Nat. Commun. **6**, 8056 (2015).
10. K. Lin, J. Xing, L. Quan, F. de Arquer, X. Gong, J. Lu, L. Xie, W. Zhao, D. Zhang, C. Yan, W. Li, X. Liu, Y. Lu, J. Kirman, E. Sargent, Q. Xiong, and Z. Wei, Nature **562**, 245 (2018).
11. T. Chiba, Y. Hayashi, H. Ebe, K. Hoshi, J. Sato, S. Sato, Y. Pu, S. Ohisa, and J. Kido, Nat. Photon. **12**, 681 (2018).
12. Z. Tan, R. Moghaddam, M. Lai, P. Docampo, R. Higler, F. Deschler, M. Price, A. Sadhanala, L. Pazos, D. Credgington, F. Hanusch, T. Bein, H. Snaith, and R. Friend, Nat. Nanotechnol. **9**, 687 (2014).
13. X. Li, M. Rui, J. Song, Z. Shen, and H. Zeng, Adv. Funct. Mater. **25**, 4929 (2015).
14. C. Motta, F. El-Mellouhi, and S. Sanvito, Sci. Rep. **5**, 12746 (2015).
15. F. Yuan, J. Xi, H. Dong, K. Xi, W. Zhang, C. Ran, B. Jiao, X. Hou, A. Y. Jen, and Z. Wu, Phys. Status Solidi RRL **12**, 1800090 (2018).
16. K. Wang, S. Sun, Ch. Zhang, W. Sun, Z. Gu, S. Xiao, and Q. Song, Mater. Chem. Front. **1**, 447 (2017).
17. D. Wiersma, *Light in Strongly Scattering and Amplifying Random Media* (University of Amsterdam, 1995).
18. A. Safdar, Y. Wang, and T. Krauss, Opt. Express **26**, A75 (2018).
19. S. Eaton, M. Lai, N. Gibson, A. Wong, L. Dou, J. Ma, L. Wang, S. Leone, and P. Yang, Proc. Natl. Acad. Sci. U. S. A. **113**, 1993 (2016).
20. P. Perumal, C. Wang, K. Boopathi, G. Haider, W. Liao, and Y. Chen, ACS Photon. **4**, 146 (2017).